High frequency repetitive transcranial magnetic stimulation alleviates cognitive deficits in 3xTg-AD mice by modulating the PI3K/Akt/GLT-1 Axis

Huan Cao [a,1], Chengchao Zuo [a,1], Zhongya Gu [a], Yaqi Huang [a], Yuyan Yang [a], Liudi Zhu [a], Yongsheng Jiang [b], Furong Wang [a,*]

[a] *Department of Neurology, Tongji Hospital, Tongji Medical College, Huazhong University of Science and Technology, No.1095 Jiefang Road, Wuhan, 430030, Hubei, China*
[b] *Cancer Center of Tongji Hospital, Tongji Medical College, Huazhong University of Science and Technology, No.1095 Jiefang Road, Wuhan, 430030, China*

ARTICLE INFO

ABSTRACT

Objective: Glutamate mediated excitotoxicity, such as oxidative stress, neuroinflammation, synaptic loss and neuronal death, is ubiquitous in Alzheimer's disease (AD). Our previous study found that 15 Hz repetitive transcranial magnetic stimulation (rTMS) could reduce cortical excitability. The purpose of this study was to explore the therapeutic effect of higher frequency rTMS on 3xTg-AD model mice and further explore the mechanisms of rTMS.

Methods: First, WT and 3xTg-AD model mice received 25 Hz rTMS treatment for 21 days. The Morris water maze test was used to evaluate the cognitive function. The levels of Aβ and neuroinflammation were assessed by ELISA and immunofluorescence. Oxidative stress was quantified by biochemical assay kits. Brain glucose metabolism was assessed by ^{18}F-FDG PET. Apoptosis was assessed by western blot and TUNEL staining. Synaptic plasticity and PI3K/Akt/GLT-1 pathway related protein expression were assessed by western blot. Next, to explore the activity of PI3K/Akt in the therapeutic effect of rTMS, 3xTg-AD model mice were given LY294002 intervention and rTMS treatment for 21 days, the experimental method was the same as before.

Results: We found that 25 Hz rTMS could improve cognitive function of 3xTg-AD model mice, reduce hippocampal Aβ1-42 levels, ameliorate oxidative stress and improve glucose metabolism. rTMS alleviated neuroinflammatory response, enhanced synaptic plasticity and reduced neuronal loss and cell apoptosis, accompanied by activation of PI3K/Akt/GLT-1 pathway. After administration of PI3K/Akt inhibitor LY294002, 25 Hz rTMS could not improve the cognitive function and reduce neuron damage of 3xTg-AD model mice, nor could it upregulate the expression of GLT-1, indicating that its therapeutic and protective effects required the involvement of PI3K/Akt/GLT-1 pathway.

Conclusion: rTMS exerts protective role for AD through regulating multiple pathological processes. Meanwhile, this study revealed the key role of PI3K/Akt/GLT-1 pathway in the treatment of AD by rTMS, which might be a new target.

1. Introduction

Alzheimer's disease (AD) is a progressive neurodegenerative disease and the most common form of dementia. The primary pathological features of AD are senile plaques (SP) formed by amyloid plaque deposition and neurofibrillary tangles (NFTs) formed by hyperphosphorylated tau. As life expectancy increases, AD has increased rapidly in the past few decades, affecting more than 11% of the population over the age of 65 and one-third of the population over the age of 85, and the prevalence of Alzheimer's disease is expected to triple by 2050 [1,2].

Four drugs have been approved by the Food And Drug Administration (FDA) to treat AD, however, these drugs can only slow the progression of AD but not actually improve patients' symptoms. Electroconvulsive therapy (ECT) has been proven to have a certain effect on AD, but it's invasive and has a lot of side effects which makes it

difficult to be widely accepted and promoted. Repetitive transcranial magnetic stimulation (rTMS) is a non-invasive neural intervention and neuromodulation technique. rTMS can affect the action potential of nerve cells and change the excitability and bioelectrical activity of neurons. Studies have shown that rTMS can reduce APP and BACE1 expression which promote amyloid beta (Aβ) generation in the hippocampus [3]. As an alternative therapy to ECT, rTMS has been applied in the clinical for a variety of neuropsychiatric disorders, including AD, depression, stroke, epilepsy, post-traumatic stress disorder, etc. [4,5]. However, the underlying neurobiological mechanisms of rTMS remain unclear.

The "amyloid cascade hypothesis" [2] suggests that accumulation of Aβ in the brain leads to tau hyperphosphorylation and neurofibrillary tangles. New evidence suggests that, in addition to Aβ accumulation, glutamate-induced excitatory toxicity and reactive oxygen species (ROS) -mediated oxidative stress are also prominent early pathological changes of AD [6]. Consistent with the hormesis paradigm [7], excessive accumulation of extracellular glutamate leads to overactivation of N-methyl-D-aspartic acid receptor (NMDA), calcium influx, mitochondrial dysfunction, oxidative stress, energy metabolism disorders, neuroinflammatory response, synapse loss and neuronal death [8–10]. The clearance of glutamate in the synaptic cleft is mainly through excitatory amino-acid transporter 2/glutamate transporter 1 (EAAT2: Human/GLT-1: Rodents) expressed in astrocytes. Aβ-dependent pathological reduction of GLT-1 was observed in the early stage of AD before plaque formation and the onset of obvious symptoms. Zott et al. [11] found that extracellular glutamate accumulation and excitatory toxicity could be reduced by upregulating GLT-1 expression. Therefore, regulating GLT-1 expression may be an effective way to prevent or delay AD related pathological changes.

In ischemic and neurodegenerative diseases, phosphatidylinositol 3-kinase (PI3K)/protein kinase B (PKB/Akt) has been shown to increase glutamate clearance by upregulating GLT-1 expression [12,13]. PI3K/Akt signaling pathway plays an important role in physiological processes such as neuroplasticity [14,15], cell survival, glucose metabolism [16,17], and mitochondrial function and oxidative stress [18, 19]. Activation of PI3K/Akt pathway can also inhibit Aβ1-42 production by modulation BACE1-mediated cleavage of APP in SweAPP N2a cells [20]. Study showed that brain-derived neurotrophic factor (BDNF) can bind to tropomyosin receptor kinase B (TrkB) to activate the PI3K/Akt pathway, protect neurons and prevent cell apoptosis [21]. Our previous studies suggested that, in depression model mice, rTMS could change the excitability of cortical pyramidal cells [22], increase the expression of BDNF and enhance synaptic plasticity and neurogenesis [23]; in 3xTg-AD model mice, rTMS could also reduce the cortical excitability by facilitating BK channels and decrease the levels of Aβ1-42, besides, the therapeutic effect of 15 Hz rTMS was better than that of 10 Hz rTMS [24]. Therefore, we speculate that high frequency rTMS may reduce the excitotoxic damage of glutamate, such as oxidative stress, energy metabolism disorders, neuroinflammation, synaptic loss and neuronal death, by upregulating GLT-1 expression via activating the PI3K/Akt.

In this study, we treated 6-8 month-old WT and 3xTg-AD mice with 25 Hz rTMS for 21 days to observe the neuroprotective effect of rTMS on 3xTg-AD mice and explored the role of PI3K/Akt/GLT-1 pathway in rTMS treatment. We found that, for 3xTg-AD mice, 25 Hz rTMS improved cognitive function, reduced Aβ1-42 levels, alleviated oxidative stress and neuroinflammatory response, enhanced energy metabolism and synaptic plasticity, reduced neuron loss, as well as increased PI3K/Akt activity and GLT-1 expression; while for 3xTg-AD mice treated with PI3K specific inhibitor LY294002, rTMS treatment could not improve the cognitive function, reduce Aβ1-42 levels and neuronal loss, nor increase GLT-1 expression. Therefore, we conclud that 25 Hz rTMS has multiple protective effects on 3xTg-AD mice and its therapeutic effects require the involvement of PI3K/Akt/GLT-1 pathway.

2. Materials and methods

2.1. Animals

Homozygous 3xTg-AD mice (PS1m146v/APPswe/TauP301L) purchased from Jackson Laboratory were used. The wild type mice (WT) have the same background (hybrid progeny of 129S1/SvIm and C57BL/6 mice). The mice were 6–8 months old at the beginning of the experiment. They were group-housed (3–4 mice per cage) under controlled temperature and humidity (23 ± 2 °C, 60–70%, 12-h light/dark cycle) with free access to food and water. All animal experiments were conducted in accordance with the guidelines approved by the Committee on the Ethics of Animal Experiments and the Institutional Animal Care and Use Committee at Tongji Medical College, Huazhong University of Science and Technology.

The experiment consisted of two stages. In the first stage, the mice were randomly divided into four groups: control + sham-rTMS、control + rTMS、3xTg + sham-rTMS、3xTg + rTMS. In the second stage, the mice were also randomly divided into four groups: 3xTg + vehicle + sham-rTMS, 3xTg + vehicle + rTMS, 3xTg + LY294002+sham-rTMS, 3xTg + LY294002+rTMS.

2.2. rTMS and drug administration

rTMS was administered with a magnetic stimulator (Magstim Rapid2, Magstim Company Ltd, Whitland, UK). Mice in the rTMS group were gently held by hand so that the skull of the left dorsolateral prefrontal lobe was attached to the central intersection of a small figure-eight coil and received 1000 stimuli per day. The stimulus waveform was biphasic. Stimulation comprised 10 trains of 100 pulses delivered at 25 Hz (4 s each train) with an intertrain interval of 25 s. The intensity of the pulse was 60% of the maximum output power of the machine. The mice in the sham-rTMS group were handled in a similar way to those treated with rTMS, hearing a 25-Hz click but not being stimulated. Both stages of rTMS treatment lasted for 28 days.

LY294002 (Selleck, USA) injection were performed as described [25]. LY294002 is a specific PI3K inhibitor that can inhibit the activity of PI3K/Akt and can cross the blood-brain barrier. According to the drug instructions and literature reports, 5% DMSO, 30% PEG300 and 10% Tween 80 were used to dissolve the drug successively, finally, the volume was fixed with ultra-pure water. Mice were intraperitoneal injection at 9:00 a.m. daily for 21 days, the drug dose was 25 mg/kg, the volume was 0.1 ml/10g. Control mice received the same volume of solvent. In the second stage, rTMS treatment was administered 1 h after drug injection.

2.3. Morris water maze (MWM) test

The MWM test was performed in a plastic cylindrical tank (1.5 m in diameter and 0.4 m high). The container was filled with water (23 ± 2 °C) dissolved in powdered milk to make it opaque. Four objects of different colors and shapes were pasted on the curtain as external geographical clues to represent four different directions. A transparent circular platform (10 cm in diameter) was placed in the center of the southeast quadrant, approximately 1 cm below the surface of the water. During five days of acquired training, the mice were placed in the water facing the wall of the pool at four different locations each day, according to a set of semirandomly selected starting positions [26], the time it took for the mice to reach the platform was recorded. If the mouse failed to find the platform within 60 s, the latency was recorded as 60 s and the mouse was guided to the platform where it remained for 15 s. On the seventh day, for the probe trial, the platform was removed and each mouse was released from the northeast quadrant. The percentage of time swimming in the target quadrant within 60 s was recorded. The performance and swimming trajectory of the mice were automatically recorded and analyzed by animal behavior analysis software

(ANY-MAZE, Stoelting, U.S.A.).

2.4. ^{18}F-FDG PET

PET acquisitions were obtained by the small animal PET scanner (TransPET®BioCaliburn® LH, China). The mice were fasted with free access to water on the day before the experiment. For the PET procedures, under 2% isoflurane anesthesia, the mice were injected 200 ± 10μCi ^{18}F-FDG via the caudal vein, the head scan of the mice was performed 57 min after injection for 10 min. After acquisition, images were reconstructed for analysis. Regions of interest (ROI) were drawn and the standard uptake value (SUV) of each ROI was calculated.

2.5. Tissue preparation

Mice were deeply anesthetized with sodium pentobarbital and perfused transcardially with 0.1 M phosphate-buffered saline (PBS). After that, half of the mice were decapitated, the hippocampus of the brain was quickly separated on ice and dipped into liquid nitrogen, then maintained at −80 °C until use. The other mice were then perfused transcardially with 4% paraformaldehyde, the whole brain was removed and post-fixed in 4% paraformaldehyde followed by gradient dehydration. Serial coronal frozen sections (12 μm thick) were cut using a cryostat (CM1950, Leica Biosystems, Wetzlar, Germany) and stored at −80 °C.

2.6. Enzyme-linked immunosorbent assay (ELISA)

The quantitatively analyzed of IL-6, IL-1β, TNF-α (Cusabio, China) and Aβ1-42 (DAB142, R&D Systems) in the hippocampus was carried out using ELISA kit according to the manufacturer's instructions. The concentration was calculated according to the corresponding standard curve. Duplication was set for each sample.

2.7. Oxidative stress measures

2.7.1. Reactive oxygen species (ROS)
Commercial kits (HR8821, biolab, Beijing) were used to measure the levels of ROS. Fresh hippocampus tissues were homogenized with buffer and centrifuged at 100 g at 4 °C for 3 min. The supernatants were collected. 200 μl supernatant and 2 μl DHE probe were added into the black 96-well plate and incubated for 30 min under dark conditions. According to the instructions, the fluorescence intensity was detected in the dark at 488–535/610 nm (excitation/emission). The protein concentration of the supernatant was determined using bicinchoninic acid assay kit.

2.7.2. Malondialdehyde (MDA)
The MDA content in the hippocampal tissue was determined using the commercial kit (BC0025, Solarbio, China) following manufacturer's protocol. Fresh hippocampus tissues were homogenized with buffer and centrifuged at 8000 g at 4 °C for 10 min. The supernatants were collected. After adding detection reagents in sequence, the suspension was incubated in the water at 100 °C for 60min, cooled on the ice, and then centrifuged at 10000g at room temperature (RT) for 10min. The absorbance of each sample at 450 nm, 532 nm and 600 nm was measured. The MDA content was calculated by formula and normalized to the mass of sample.

2.7.3. Superoxide dismutase (SOD)
The SOD content in the hippocampal tissue was determined using the commercial kit (BC0175, Solarbio, China) following manufacturer's protocol. Fresh hippocampus tissues were homogenized with buffer and centrifuged at 8000 g at 4 °C for 10 min. The supernatants were collected. After adding samples and detection reagents in sequence, the suspension was incubated in the water at 37 °C for 30min. The

absorbance of each sample at 560 nm was measured. The SOD content was calculated by formula and normalized to the mass of sample.

2.7.4. Glutathione (GSH)
The GSH content in the hippocampal tissue was determined using the commercial kit (BC1175, Solarbio, China) following manufacturer's protocol. Fresh hippocampus tissues were homogenized with buffer and centrifuged at 8000 rpm at 4 °C for 10 min. Dissolve standard to different concentrations and make standard curves. The absorbance of each sample at 412 nm was measured. The GSH content was determined according to the standard curve.

2.8. Western blotting

Hippocampus tissues were homogenized on ice for 30 min and centrifuged at 12000 rpm at 4 °C for 15 min. The supernatants were collected for follow-up measurement. Protein concentration was determined using BCA method. Equal amounts of protein (25 μg) were separated by sodium dodecyl sulfate polyacrylamide gel electrophoresis (SDS-PAGE) and transferred to nitrocellulose membranes. After blocked in 5% nonfat milk/tris-buffered saline with Tween 20 (TBST) or 5% bovine serum albumin (BSA) at RT for 1 h, the membranes were incubated overnight with primary antibodies including anti-GLT-1 (1:1000; Millipore), anti-PSD-95 (1:1000; Abcam), anti-SYP (1:1000; Abcam), anti-NR1 (1:1000; Cell Signaling Technology), anti-NR2A (1:1000; Cell Signaling Technology), anti-NR2B (1:1000; Cell Signaling Technology), anti-PI3K (1:1000; Abcam), anti-Akt (1:1000; Cell Signaling Technology), anti-p-Akt (1:1000; Cell Signaling Technology), anti-Bax (1:1000; Abcam), anti-Bcl-2 (1:2000; Abcam) and anti-β-actin (1:500; Boster). Then the membranes were washed with TBST for 3 × 10 min and incubated with horseradish peroxidase (HRP)-conjugated secondary antibody (1:5000; Servicebio) at RT for 1 h. Next, the membranes were washed for 3 × 10 min and the immunoreactive bands were detected by the Bio-Rad Chemi Doc XRS + imaging system. Densitometric analysis was analyzed with the use of ImageJ software.

2.9. Immunofluorescence

Brain sections were rinsed with PBS for 10 min, permeabilized with PBS containing 3% H_2O_2 and 0.25% Triton X-100 for 20 min and blocked in 5% BSA at RT for 2 h. Next, the sections were incubated with primary antibodies including anti-Iba1 (1:1000; Wako), anti-CD68 (1:200; Abcam), 6E10 (1:1000; Biolegend) and anti-NeuN (1:1000; Millipore) at 4 °C for overnight (at least 16 h). Then, the sections were rinsed with Tris-Buffer saline (TBS) for 3 × 10 min and incubated with corresponding secondary antibodies including Alexa Fluor 594 Donkey Anti-Mouse IgG (1:1000; Abcam), Alexa Fluor 488 Donkey Anti-Rabbit IgG (1:1000; Abcam) and Alexa Fluor 647 Donkey Anti-Rat IgG (1:1000, Abcam) for 1 h at RT in darkness. Finally, sections were washed with Tris-Buffer saline (TBS) for 3 × 10 min and stained with 4,6-diamidino-2-phenylindole (DAPI) (10 μg/mL, Sigma-Aldrich) for 10 min at RT. Images were acquired using a laser scanning confocal microscope (FV1000; Olympus, Tokyo, Japan) and analyzed by Image J software.

2.10. TUNEL staining

TUNEL (Cell Death Detection Kit, Roche, Basel, Switzerland) staining was performed according to the instructions. Briefly, after antigen retrieval, brain sections were incubated with 50 μl TUNEL reaction mixture at 37 °C in darkness for 1 h. Images were acquired using a laser scanning confocal microscope (FV1000; Olympus, Tokyo, Japan).

2.11. Statistical analysis

All statistical analyses were performed by SPSS 19.0 (IBM, USA). Significant differences between groups were analyzed by Student's t-test

or two-way ANOVA followed by the Tukey test. $p < 0.05$ was considered to be significant. The data were presented as the mean ± SEM.

3. Results

1. Effects of rTMS on cognitive function and levels of Aβ1-42, GLT-1 in 3xTg-AD mice

To explore the therapeutic effects of 25 Hz rTMS on 3xTg-AD mice, mice were divided into 4 groups: control + sham-rTMS、control + rTMS、3xTg + sham-rTMS、3xTg + rTMS. In the MWM test, on the fifth day of the acquired training period, the escape latency of the 3xTg + sham-rTMS group was significantly longer than that of the control + sham-rTMS group ($p < 0.001$); compared with the 3xTg + sham-rTMS

group, the escape latency of 3xTg + rTMS group was significantly shorter ($p < 0.001$) (Fig. 1A); there was no significant difference between the control + sham-rTMS group and the control + rTMS group ($p > 0.05$) (Fig. 1A). In the probe trial period, the percentage of swimming time in the target quadrant of mice in 3xTg + sham-rTMS group was significantly lower than that in control + sham-rTMS group ($p < 0.01$) (Fig. 1B); rTMS significantly increased the percentage of swimming time in the target quadrant in 3xTg-AD mice ($p < 0.001$) (Fig. 1B), while rTMS had no significant effect on the control group ($p > 0.05$) (Fig. 1B). Compared with the 3xTg + sham-rTMS group, the level of Aβ1-42 in the hippocampus of mice in 3xTg + rTMS group was significantly decreased ($p < 0.05$) (Fig. 1D and E), which is consistent with our previous conclusions. Since Aβ can reduce GLT-1 expression and induce glutamate-induced excitatory toxicity, we detected the expression level of GLT-1.
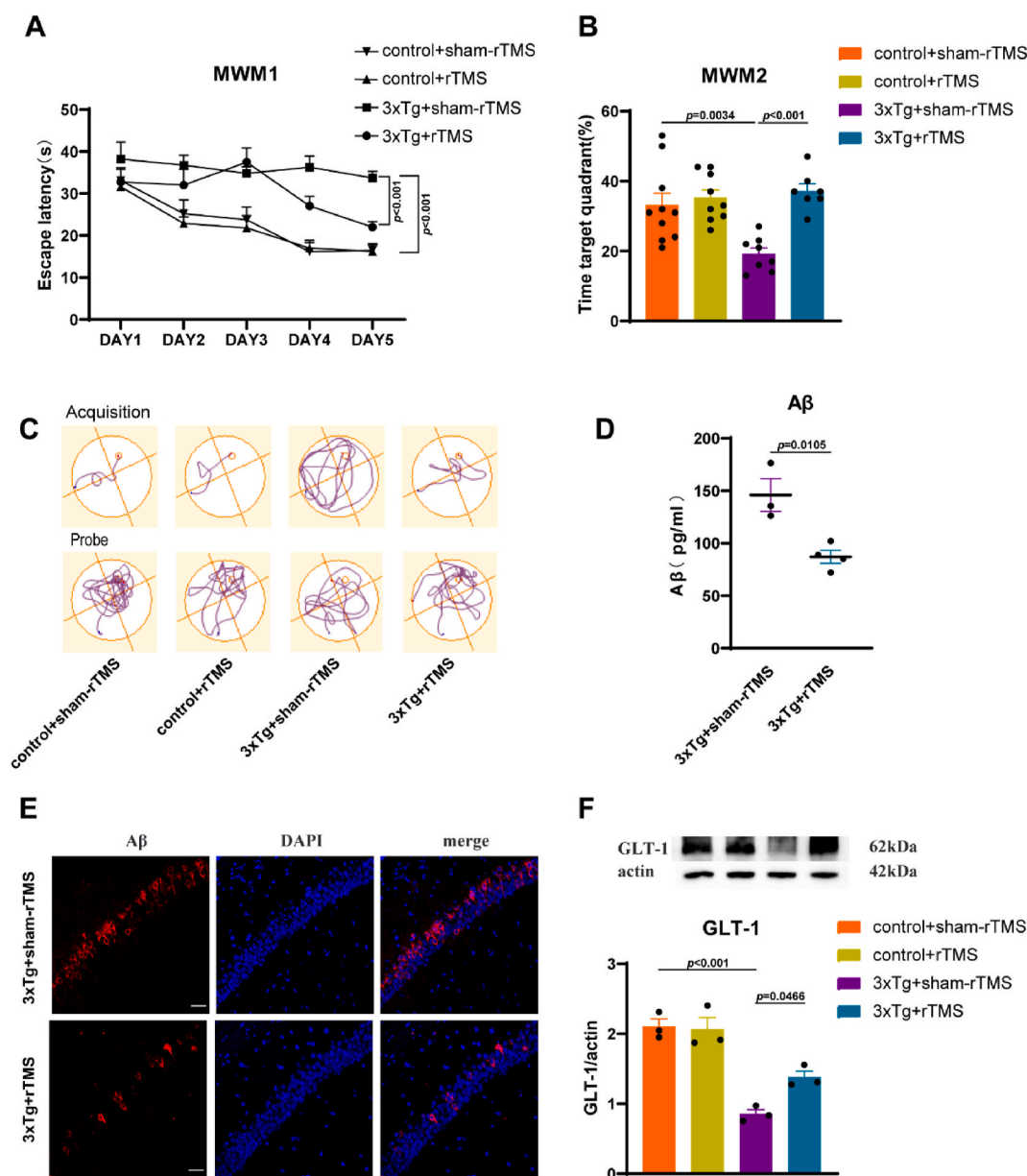
Fig. 1. rTMS improved the spatial learning and memory abilities of 3xTg-AD mice, reduced Aβ1-42 levels and increased GLT-1 expression. **A** The escape latency during the acquired training period. **B** The percentage of swimming time in the target quadrant during the probe trial period. **C** Representative swimming trajectory diagram of mice in the acquired training period and the probe trial period. **D** Hippocampal Aβ1-42 levels detected by ELISA. **E** Representative immunofluorescent staining images of Aβ (red) with DAPI (blue) in the CA1 region of hippocampus. Scale bar = 100 μm. **F** Representative western blot images and quantitative analysis of GLT-1 in the hippocampus. All data were represented as mean ± SEM and analyzed by T test or two-way ANOVA with Tukey's post hoc test. (For interpretation of the references to color in this figure legend, the reader is referred to the Web version of this article.)

Compared with the control + sham-rTMS group, the expression of GLT-1 in the hippocampus of 3xTg + sham-rTMS group was significantly decreased ($p < 0.001$) (Fig. 1F). After rTMS treatment, the expression of GLT-1 in 3xTg + rTMS group was significantly higher than that in 3xTg + sham-rTMS group ($p < 0.05$) (Fig. 1F). There was no significant difference in hippocampal GLT-1 expression between control + sham-rTMS group and control + rTMS group ($p > 0.05$) (Fig. 1F).

2. Effects of rTMS on the level of oxidative stress and brain glucose metabolism of 3xTg-AD mice

We detected oxidative stress-related indicators in the hippocampus. The results showed that the levels of ROS in the 3xTg + sham-rTMS group was significantly higher than that in the control + sham-rTMS group ($p < 0.01$) (Fig. 2A); after rTMS treatment, ROS levels in the 3xTg
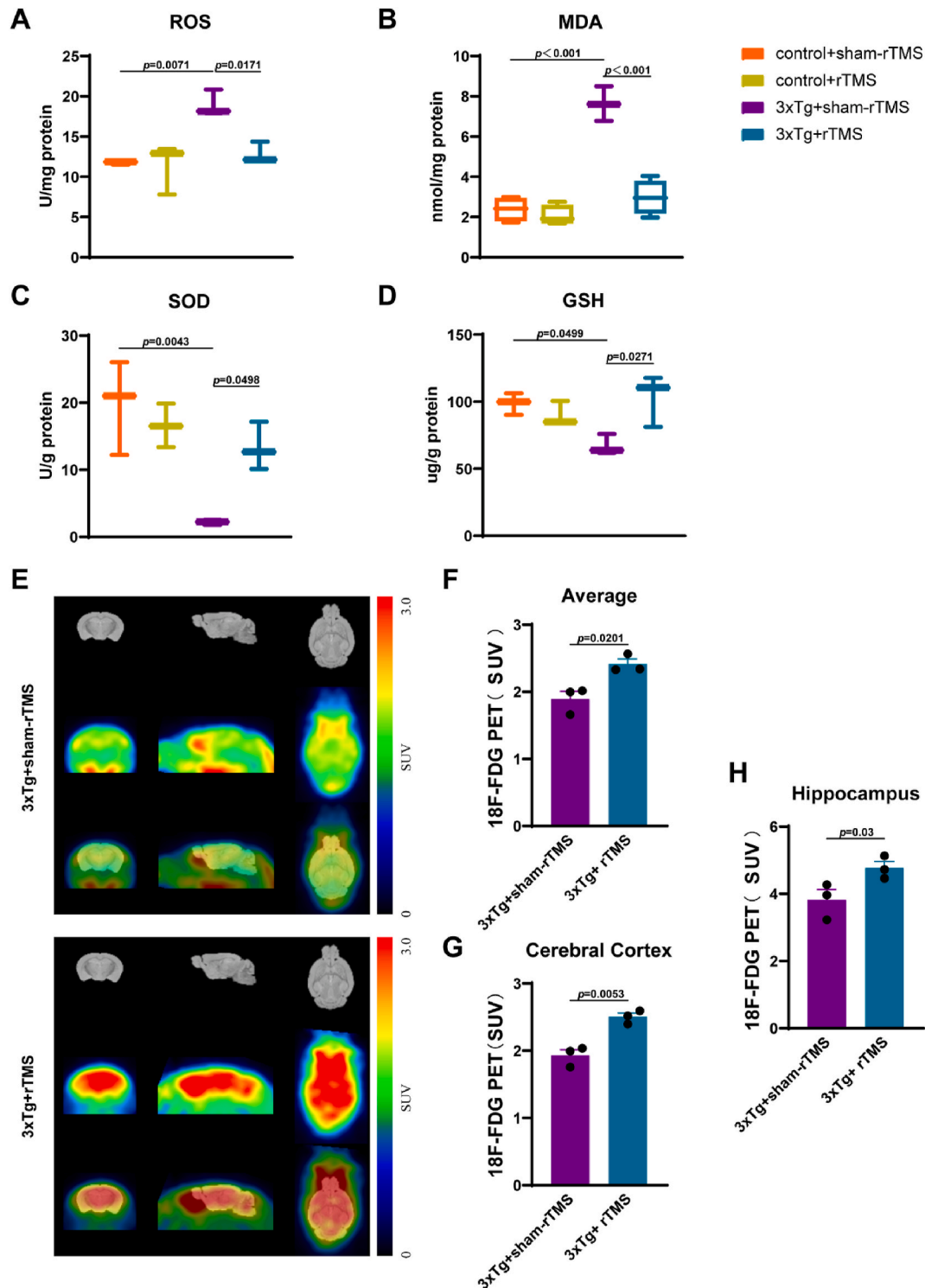
Fig. 2. rTMS treatment reduced the level of oxidative stress and improved brain glucose metabolism. **A-D** The level of ROS (**A**), MDA (**B**), SOD (**C**), GSH (**D**) detected by ELISA in the CA1 region of hippocampus (n = 3–4). **E** ^{18}F-FDG PET image of mouse brain tissue. **F** Statistics of average SUV value. **G** Statistics of cortex SUV values. **H** Statistics of hippocampus SUV values. All data were represented as mean ± SEM and analyzed by T test or two-way ANOVA with Tukey's post hoc test.

+ rTMS group was significantly lower than that in the 3xTg + sham-rTMS group ($p < 0.05$) (Fig. 2A). Compared with control + sham-rTMS group, the level of MDA in the hippocampus of 3xTg + sham-rTMS group was significantly increased ($p < 0.001$) (Fig. 2B), while rTMS decreased the level of MDA in the hippocampus of 3xTg-AD mice ($p < 0.001$) (Fig. 2B). Compared with control + sham-rTMS group, SOD ($p < 0.01$) (Fig. 2C) and GSH ($p < 0.05$) (Fig. 2D) levels in the hippocampus of 3xTg + sham-rTMS group were significantly decreased, rTMS significantly increased SOD and GSH levels in hippocampus of 3xTg-AD mice ($p < 0.05$) (Fig. 2C , 2D). As shown in Fig. 2, there was no significant difference in the level of oxidative stress in the hippocampus between the control + sham-rTMS group and the control + rTMS group ($p > 0.05$). Using ^{18}F-FDG PET technology, we found that rTMS significantly increased the average glucose metabolism level of brain tissue ($p < 0.05$) (Fig. 2E and F), as well as the glucose metabolism level of cortex ($p < 0.01$) (Fig. 2E and G) and hippocampus ($p < 0.05$) (Fig. 2E and H) in 3xTg-AD mice.

3. Effect of rTMS on neuroinflammation in 3xTg-AD mice

Two-way ANOVA showed no difference in the number of Iba1$^+$ microglia cell in hippocampal CA1 region among all groups ($p > 0.05$) (Fig. 3A and B). Co-labeling of CD68$^+$ and Iba1$^+$ microglia cells in immunofluorescence staining was used to detect the activation of microglia, the results showed that the ratio of CD68$^+$ Iba1$^+$ cells/Iba1$^+$ cells in hippocampal CA1 region was not significantly different between control+sham-rTMS and 3xTg + sham-rTMS groups ($p > 0.05$), 3xTg + sham-rTMS and 3xTg + rTMS groups ($p > 0.05$) (Fig. 3A and B). Immunofluorescence staining results in the hippocampal DG region showed that the number of Iba1$^+$ microglia cells ($p < 0.05$) was higher than that in control + sham-rTMS group, rTMS treatment reduced the activation level of microglia in the hippocampal DG region of 3xTg-AD mice ($p < 0.05$) (Fig. 3C and D). There was no significantly difference in the number of Iba1$^+$ microglia cell ($p > 0.05$) and the ratio of CD68$^+$ Iba1$^+$ cells ($p > 0.05$) in hippocampal DG region between control + sham-rTMS group and control + rTMS group (Fig. 3C and D).

We further measured the levels of pro-inflammatory cytokines IL-6, IL-1β and TNF-α in the hippocampus by ELISA. Compared with the control + sham-rTMS group, the levels of IL-6 ($p < 0.01$) (Fig. 3E), IL-1β ($p < 0.01$) (Fig. 3F) and TNF-α ($p < 0.01$) (Fig. 3G) in the hippocampus of 3xTg + sham-rTMS group were significantly increased, rTMS significantly decreased the levels of IL-6 ($p < 0.01$) (Fig. 3E), IL-1β ($p < 0.05$) (Fig. 3F) and TNF-α ($p < 0.001$) (Fig. 3G) in 3xTg-AD mice. In addition, rTMS reduced TNF-α levels in the hippocampus of control mice (p < 0.05) (Fig. 3G), there was no significantly difference in the levels of IL-6 (Fig. 3E) and IL-1β (Fig. 3F) between control + sham-rTMS group and control + rTMS group ($p > 0.05$).

4. Effects of rTMS on synaptic plasticity and neuronal loss in 3xTg-AD mice

Compared with the control + sham-rTMS group, the levels of synaptophysin (SYP) ($p < 0.01$) and postsynaptic density 95 (PSD-95) ($p < 0.05$) in the hippocampus of mice in 3xTg + sham-rTMS group were significantly decreased (Fig. 4B and C). After rTMS treatment, the levels of SYP ($p < 0.05$) and PSD-95 ($p < 0.05$) in the hippocampus of mice in 3xTg + rTMS group were significantly higher than those in 3xTg + sham-rTMS group (Fig. 4B and C). The levels of NR1 (p < 0.01), NR2A (p < 0.05) and NR2B (p < 0.01) were significantly decreased in the hippocampus of 3xTg-AD mice. rTMS reversed the down-regulation of NR2B level (p < 0.01), but had no significant effect on the expression of NR1 and NR2A (Fig. 4D, E, 4F). There was no significant difference in the number of NeuN$^+$ neurons in hippocampal CA1 region among the groups (Fig. 4G and H). Compared with the control + sham-rTMS group, the number of NeuN$^+$ neurons in hippocampal DG region in 3xTg+sham-TMS group was significantly reduced ($p < 0.05$) (Fig. 4G

and H), rTMS treatment increased the number of NeuN$^+$ neurons in the DG region ($p < 0.05$) (Fig. 4G and H). TUNEL staining results showed that, compared with the control + sham-rTMS group, the apoptotic cells in the hippocampus of 3xTg + sham-rTMS group increased, the ratio of Bcl-2/Bax was significantly decreased simultaneously ($p < 0.05$) (Fig. 4I and J). After rTMS treatment, the apoptotic cells in hippocampus of 3xTg-AD mice decreased and the ratio of Bcl-2/Bax was up-regulated ($p < 0.05$) (Fig. 4I and J). As shown in Fig. 4, there was no significant difference in the expression of hippocampal synapse-associated proteins and the number of neurons between control + sham-rTMS group and control + rTMS group ($p > 0.05$).

5. Effect of rTMS on the activity of PI3K/Akt

The results showed that compared with the control + sham-rTMS group, the expression of PI3K in 3xTg + sham-rTMS group was significantly reduced ($p < 0.05$), rTMS treatment increased PI3K expression, but the difference was not significant ($p > 0.05$) (Fig. 5A). rTMS had no significant effect on PI3K protein expression of control mice ($p > 0.05$) (Fig. 5A). There was no significant difference in the level of total Akt in the hippocampus among groups ($p > 0.05$) (Fig. 5C). Compared with the control + sham-rTMS group, the level of p-Akt/Akt in hippocampus of 3xTg + sham-rTMS group was significantly decreased ($p < 0.001$), rTMS treatment reversed the down-regulation of p-Akt/Akt of 3xTg-AD mice ($p < 0.001$) (Fig. 5D). There was no difference in hippocampal p-Akt/Akt levels between the control + sham-rTMS group and the control + rTMS group ($p > 0.05$) (Fig. 5D). These results suggested that rTMS treatment reversed the downregulation of PI3K/Akt activity.

6. LY294002 inhibited the activation of PI3K/Akt/GLT-1 pathway and the cognitive improvement effect by rTMS

PI3K inhibitor LY294002 was used to further explore the role of PI3K/Akt/GLT-1 pathway in rTMS treatment of 3xTg-AD mice. Mice were divided into 4 groups: 3xTg + vehicle + sham-rTMS, 3xTg + vehicle + rTMS, 3xTg + LY294002+sham-rTMS, 3xTg + LY294002+rTMS. Compared with the 3xTg + vehicle + sham-rTMS group, the protein expression of PI3K in 3xTg + vehicle + rTMS group was significantly increased ($p < 0.05$) (Fig. 6A). After LY294002 administration, there was no significant difference in PI3K protein expression between 3xTg + LY294002+sham-rTMS group and 3xTg + LY294002+rTMS group ($p > 0.05$) (Fig. 6A). ANOVA analysis showed no significant difference in the total Akt expression level between the four groups ($p > 0.05$) (Fig. 6B). Compared with 3xTg + vehicle + sham-rTMS group, the level of p-Akt/Akt in the hippocampus in 3xTg + vehicle + rTMS group was significantly increased ($p < 0.05$), while this effect of rTMS was blocked by LY294002 ($p > 0.05$) (Fig. 6C). Compared with the 3xTg + vehicle + sham-rTMS group, the level of GLT-1 in the hippocampus of 3xTg + vehicle + rTMS group was significantly increased ($p < 0.05$), while there was no significant difference in the GLT-1 expression between 3xTg + LY294002+sham-rTMS group and 3xTg + LY294002+rTMS group ($p > 0.05$) (Fig. 6D). In the MWM test, we found that on the fifth day of the acquired training period, compared with the 3xTg + vehicle + sham-rTMS group, the escape latency of mice in the 3xTg + vehicle + rTMS group was shorter. However, after the administration of LY294002, the escape latency of mice in the 3xTg + LY294002+rTMS group was not significantly different from that of mice in the 3xTg + LY294002+sham-rTMS group (Fig. 6E). In the probe trial period, the percentage of swimming time in the target quadrant of mice in the 3xTg + vehicle + rTMS group was significantly higher than that of mice in the 3xTg + vehicle + sham-rTMS group ($p < 0.05$), while there was no significant difference between the 3xTg + LY294002+rTMS group and the 3xTg + LY294002+sham-rTMS group ($p > 0.05$) (Fig. 6F).

7. LY294002 inhibited the effects of rTMS on reducing Aβ1-42 levels and neuronal loss
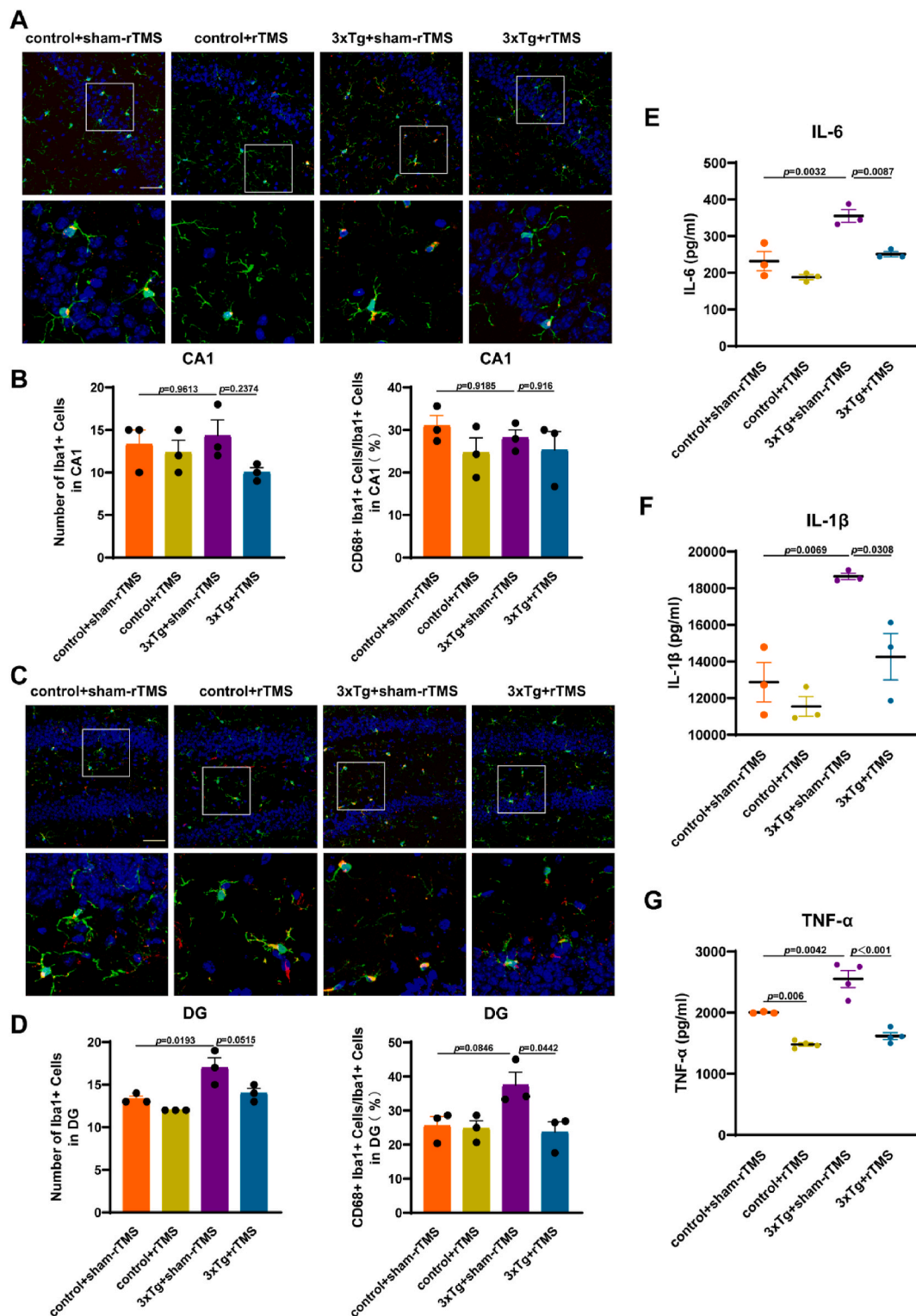
Fig. 3. rTMS reduced neuroinflammation in 3xTg-AD mice. **A** Representative immunofluorescent staining images of Iba1^{+} (green), CD68^{+} (red) with DAPI (blue) in the CA1 region of hippocampus. Scale bar = 50 μm. **B** Statistical diagram of the number of Iba1^{+} microglia cells and the ratio of CD68^{+} Iba1^{+} cells/Iba1^{+} cells in the CA1 region of hippocampus. **C** Representative immunofluorescent staining images of Iba1^{+} (green), CD68^{+} (red) with DAPI (blue) in the DG region of hippocampus. Scale bar = 50 μm. **D** Statistical diagram of the number of Iba1^{+} microglia cells and the ratio of CD68^{+} Iba1^{+} cells/Iba1^{+} cells in the DG region of hippocampus. **E-G** Hippocampal IL-6 (**E**), IL-1β (**F**) and TNF-α (**G**) levels detected by ELISA. At least 9 fluorescence microscope photos of 3 mice were included in each group for statistical analysis. All data were represented as mean ± SEM and analyzed by two-way ANOVA with Tukey's post hoc test. (For interpretation of the references to color in this figure legend, the reader is referred to the Web version of this article.)
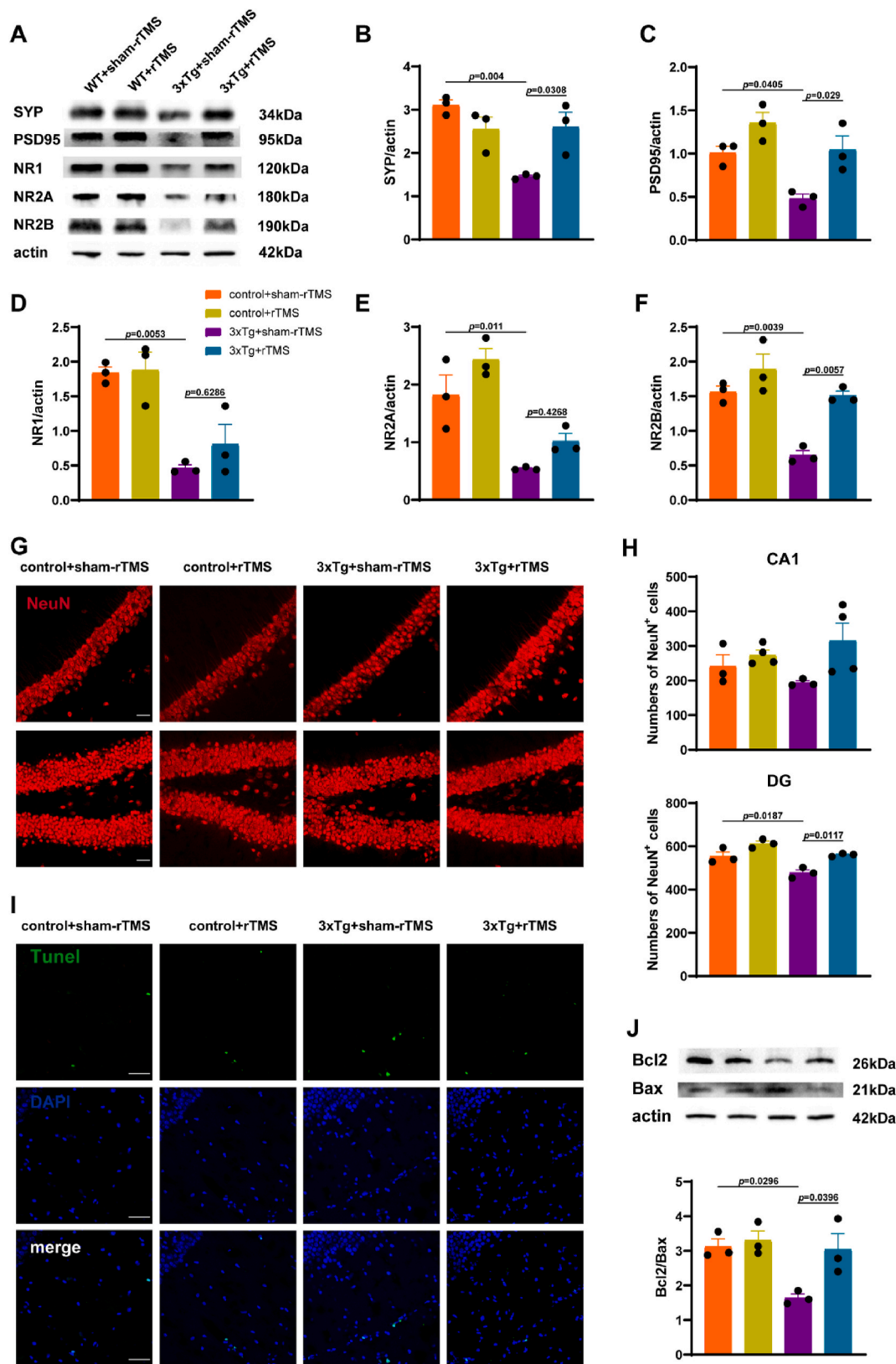
Fig. 4. rTMS restored synaptic plasticity and reduced neuron loss in 3xTg-AD mice. **A** Representative western blot images of SYP, PSD-95, NR1, NR2A and NR2B in the hippocampus. **B–F** Quantitative analysis of SYP (**B**), PSD-95 (**C**), NR1 (**D**), NR2A (**E**) and NR2B (**F**) in the hippocampus. **G** Representative immunofluorescent staining of NeuN $^{+}$ cells (red) in the CA1 and DG region of hippocampus. Scale bar = 100 μm. **H** Statistical diagram of NeuN $^{+}$ cells in hippocampal CA1 and DG region. **I** Representative immunofluorescent staining of Tunel (green) with DAPI (blue) in the hippocampus. Scale bar = 50 μm. **J** Representative western blot images and quantitative analysis of Bcl-2/Bax in the hippocampus. At least 9 fluorescence microscope photos of 3 mice were included in each group for statistical analysis. All data were represented as mean ± SEM and analyzed by two-way ANOVA with Tukey's post hoc test. (For interpretation of the references to color in this figure legend, the reader is referred to the Web version of this article.)
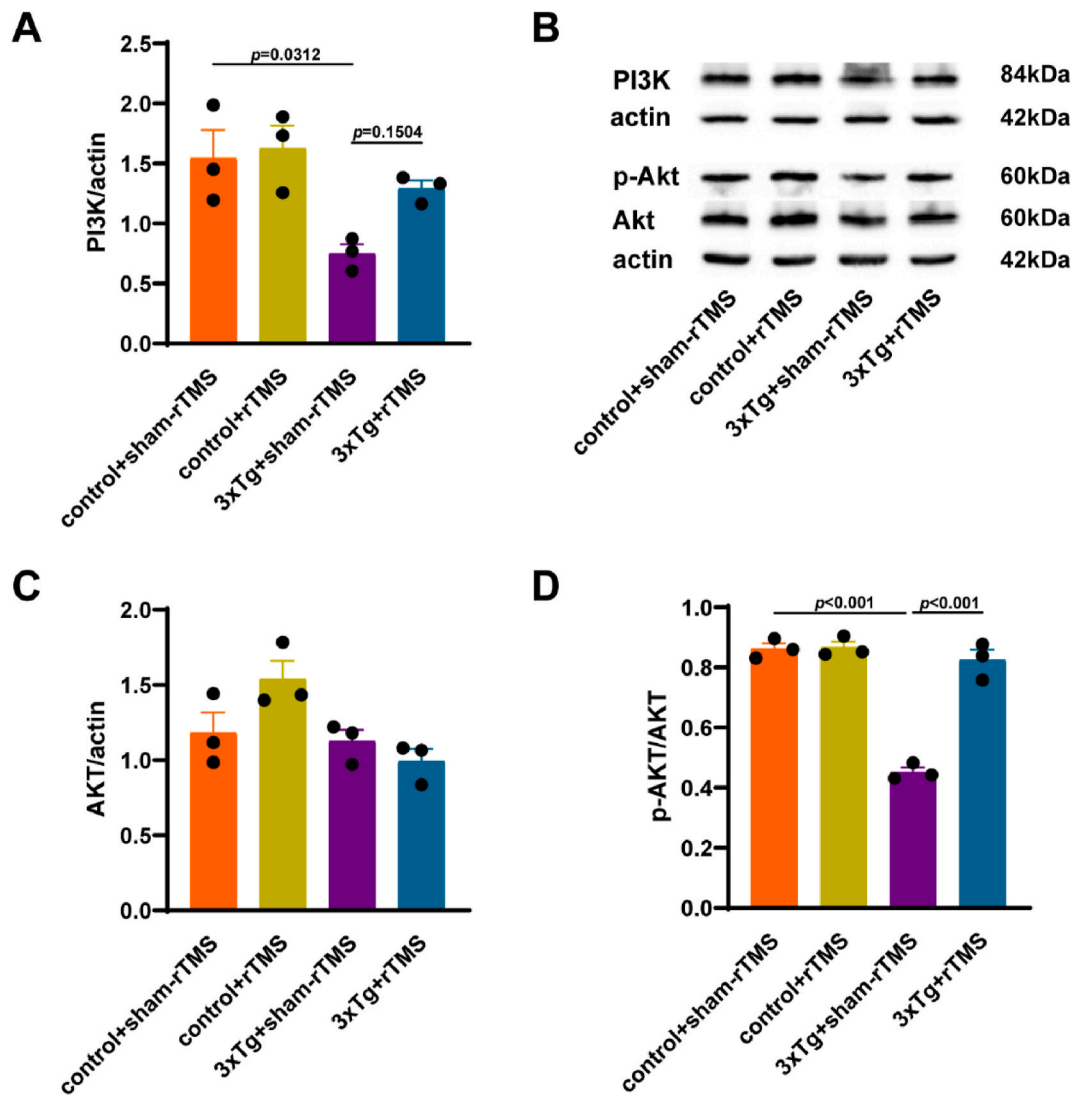
Fig. 5. Effects of rTMS treatment on PI3K/Akt activity in 3xTg-AD mice. **A** Quantitative analysis of PI3K in the hippocampus. **B** Representative western blot images of PI3K, Akt and p-Akt in the hippocampus. **C** Quantitative analysis of Akt in the hippocampus. **D** Quantitative analysis of p-Akt/Akt in the hippocampus. All data were represented as mean ± SEM and analyzed by two-way ANOVA with Tukey's post hoc test.

As shown in Fig. 7, hippocampal Aβ1-42 levels in 3xTg + vehicle + rTMS group was significantly lower than that in 3xTg + vehicle + sham-rTMS group ($p < 0.01$) (Fig. 7A and B). rTMS did not decrease the levels of Aβ1-42 in the hippocampus of 3xTg-AD mice after LY294002 administration ($p > 0.05$) (Fig. 7A and B). Compared with the 3xTg + vehicle + sham-rTMS group, the number of NeuN$^+$ neurons in hippocampal CA1 ($p < 0.01$) (Fig. 7C and D) and DG ($p < 0.05$) (Fig. 7C, E) regions in the 3xTg + vehicle + rTMS group was significantly increased, there was no significant difference in the number of NeuN$^+$ neurons between 3xTg+LY294002+sham-rTMS group and 3xTg + LY294002+rTMS group ($p > 0.05$). TUNEL staining results showed that compared with the 3xTg + vehicle + sham-rTMS group, the apoptotic cells in the hippocampus of 3xTg + vehicle + rTMS group increased and the ratio of Bcl-2/Bax reduced ($p < 0.05$) (Fig. 7F and G). There was no significant difference in Bcl-2/Bax ratio between 3xTg + LY294002+-sham-rTMS group and 3xTg + LY294002+rTMS group ($p > 0.05$) (Fig. 7G).

4. Discussion

The high morbidity and disability rate of AD make the burden of society and family increase continuously, prevention and treatment of

AD has become a major public health problem worldwide. Our previous study showed that compared with 10 Hz rTMS, 15 Hz rTMS significantly improved cognitive function, regulated cortical excitability and enhanced long-term potentiation (LTP) in 3xTg-AD mice [24]. In this study, we explored higher frequency of rTMS and found that 25 Hz rTMS could not only improve spatial learning and memory ability of 3xTg-AD mice, decrease hippocampal Aβ1-42 levels, but also ameliorate oxidative stress and glucose metabolism, alleviate neuroinflammatory response, restore synaptic plasticity, reduce neuron loss and cell apoptosis. Moreover, it was accompanied by activation of PI3K/Akt pathway and up-regulation of GLT-1 expression. However, after administration of PI3K specific inhibitor LY294002 to inhibit PI3K/Akt activity, 25 Hz rTMS could not improve the cognitive function, decrease Aβ1-42 levels, reduce neuronal loss and cell apoptosis in 3xTg-AD mice, and could not restore the expression level of GLT-1 simultaneously. Therefore, we conclud that 25 Hz rTMS may exert multiple neuroprotective effects on 3xTg-AD mice by regulating the PI3K/Akt/GLT-1 signaling pathway.

Inhibition of glutamate reuptake by Aβ leads to extracellular glutamate accumulation and extrasynaptic NMDARs (eNMDARs) over-activation, which have a much higher permeability for Ca$^+$ [27]. Massive calcium influx leads to mitochondrial dysfunction, such as
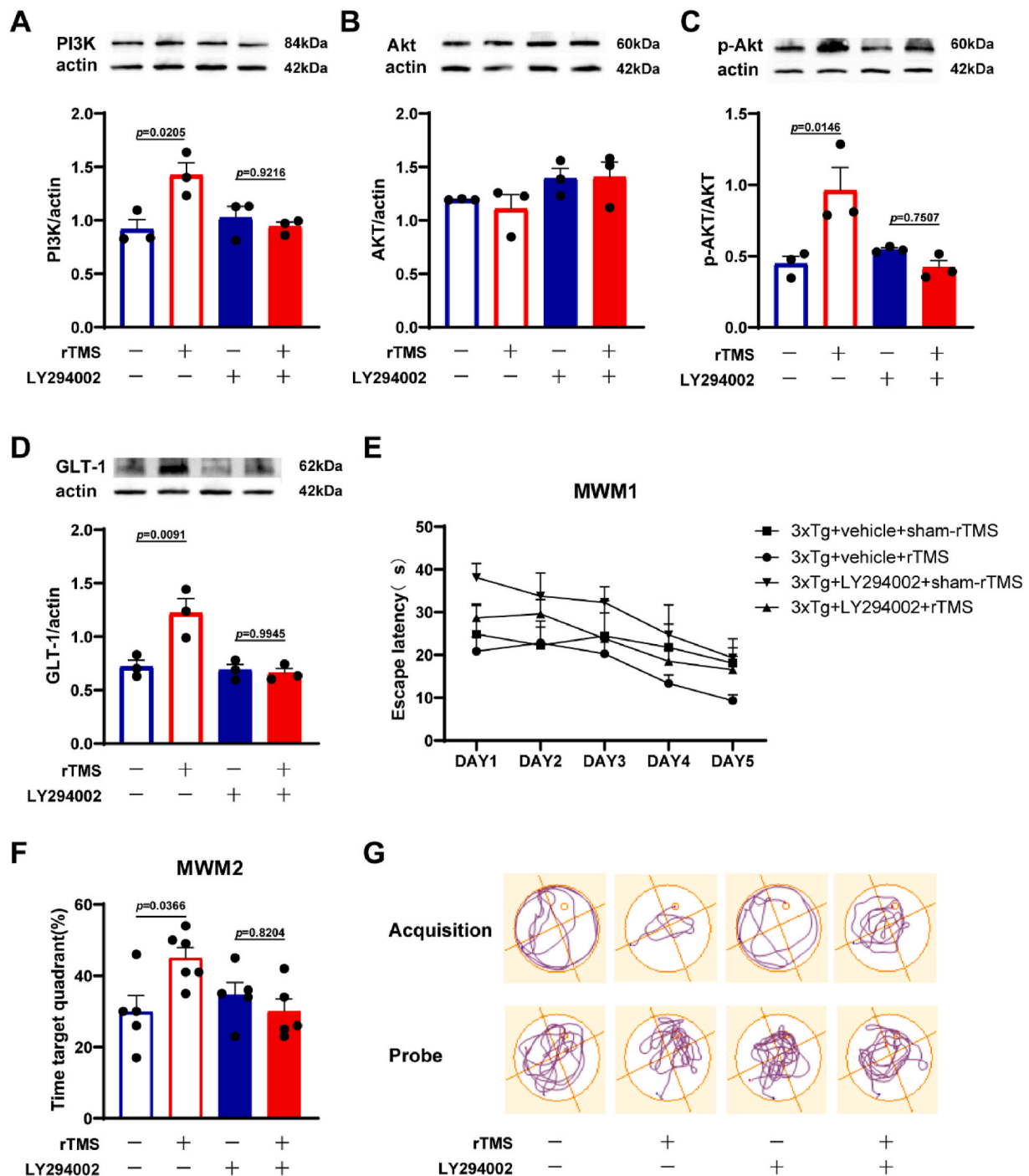
Fig. 6. Effects of LY294002 intervention on the activation of PI3K/Akt/GLT-1 pathway and the improvement of spatial learning and memory in 3xTg-AD mice by rTMS. **A** Representative western blot images and quantitative analysis of PI3K in the hippocampus. **B** Representative western blot images and quantitative analysis of Akt in the hippocampus. **C** Representative western blot images and quantitative analysis of p-Akt/Akt in the hippocampus. **D** Representative western blot images and quantitative analysis of GLT-1 in the hippocampus. **E** The escape latency during the acquired training period. **F** The percentage of swimming time in the target quadrant during the probe trial period. **G** Representative swimming trajectory diagram of mice in the acquired training period and the probe trial period. All data were represented as mean ± SEM and analyzed by two-way ANOVA with Tukey's post hoc test.

increased ROS production and decreased ATP production, resulting in oxidative stress, energy metabolism disorders, inflammatory response, as well as severe synaptic loss and apoptosis [27–29]. Oxidative stress levels were significantly higher in the brains of MCI and AD patients compared to healthy people [30]. Excess production of ROS means extensive oxidative damage to DNA, RNA, proteins, lipids and depletion of endogenous antioxidant defense systems, especially in the brain regions most associated with AD, such as the hippocampus and cortex [31,

32]. MDA is a decomposition product of lipid peroxides, which can reflect the level of lipid peroxidation and indirectly reflect the degree of cell damage [33]. SOD is a major antioxidant in antioxidant enzyme system, its content reflects the ability of scavenging oxygen free radicals in the body [34]. GSH which belongs to non-antioxidant enzyme system can remove excess free radicals and ROS in the body to prevent cell oxidative stress damage. This study found that the level of oxidative stress in hippocampus of 3xTg-AD mice increased, which was consistent
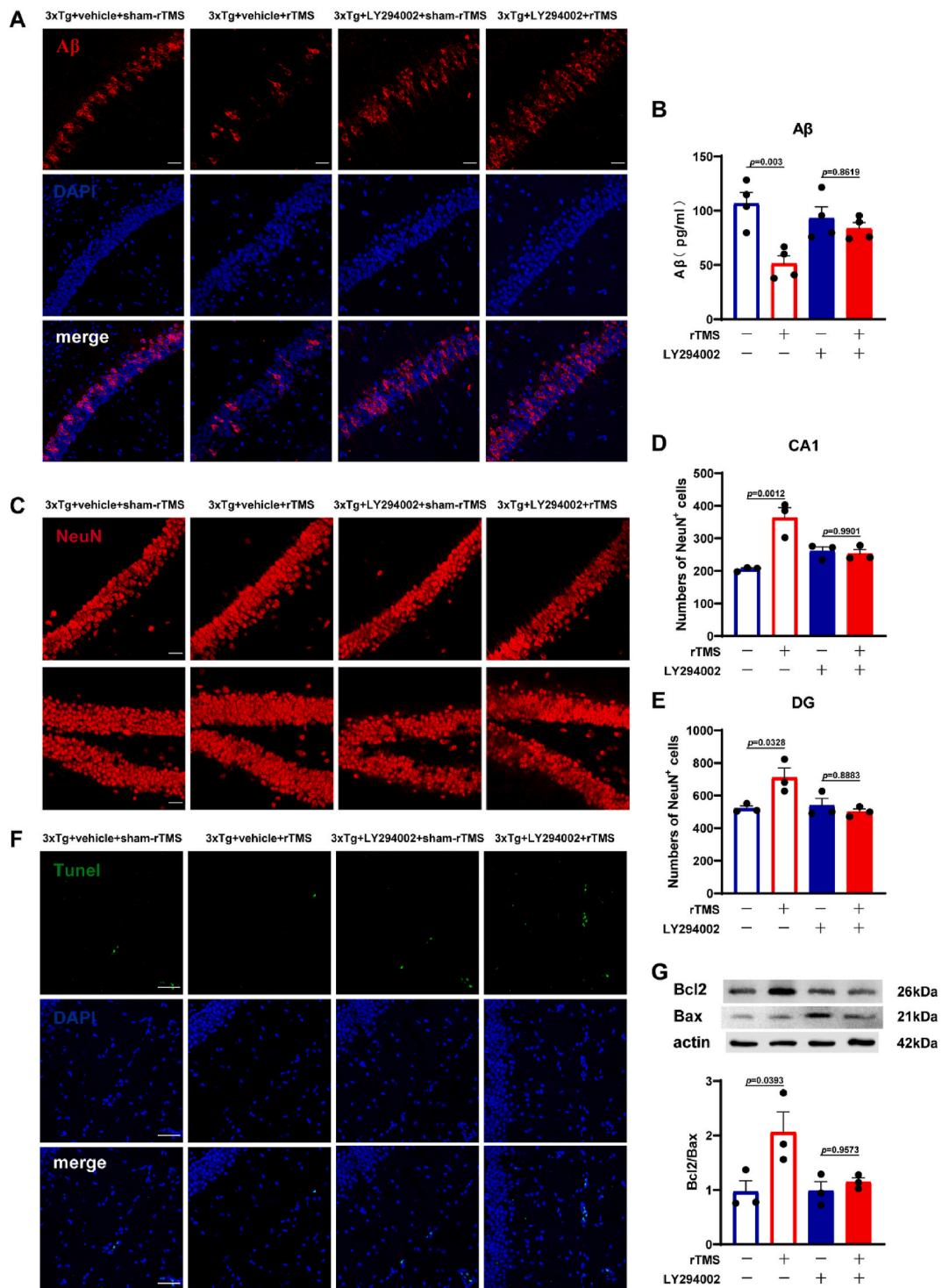
Fig. 7. Effects of LY294002 intervention on reducing Aβ1-42 levels and neuron loss by rTMS in 3xTg-AD mice. **A** Representative immunofluorescent staining images of Aβ (red) with DAPI (blue) in the CA1 region of hippocampus. Scale bar = 100 μm. **B** Quantitative statistics of Aβ1-42 levels in the hippocampus detected by ELISA. **C** Representative immunofluorescent staining of NeuN$^+$ cells (red) in the CA1 and DG region of hippocampus. Scale bar = 100 μm. **D-E** Statistical diagram of NeuN$^+$ cells in hippocampal CA1 (**D**) and DG (**E**) region. **F** Representative immunofluorescent staining of Tunel (green) with DAPI (blue) in the hippocampus. Scale bar = 50 μm. **G** Representative western blot images and quantitative analysis of Bcl-2/Bax in the hippocampus. At least 9 fluorescence microscope photos of 3 mice were included in each group for statistical analysis. All data were represented as mean ± SEM and analyzed by two-way ANOVA with Tukey's post hoc test. (For interpretation of the references to color in this figure legend, the reader is referred to the Web version of this article.)

with previous studies. Low levels of BDNF can lead to a persistent state of oxidative stress, while restoring BDNF level can restore Nrf2 function and activate defense mechanism [7,35]. Our previous study showed that rTMS can up-regulate the expression of BDNF. In this study, it was found that rTMS significantly alleviated oxidative stress through reducing the

levels of ROS, MDA, and increasing the levels of SOD and GSH in the hippocampus of 3xTg-AD mice.

Brain is the most abundant organ for human energy metabolism. In a resting and waking state, it consumes about 20% of the body's oxygen and 25% of glucose [36]. Mitochondria is the energy-supplying and

metabolism centers of cell. Sugar uptake and metabolism have been reduced in the early stage of AD [37]. Positron emission tomography using 18F-fluorodeoxyglucose as a tracer has become the most common and effective method for measuring brain energy metabolism and can detect subtle changes in glucose metabolism in mouse brain tissue [38]. FDG-PET studies have shown that the glucose metabolism in the brain tissue of AD patients is continuously and progressively decreased, and the degree of decrease is related to the severity of symptoms; in addition, the decrease in regional brain glucose metabolism shown by FDG-PET is also accompanied by a decrease in synaptic activity and density in corresponding regions, suggesting that the decreased regional selective brain glucose metabolism in AD patients may be associated with specific cognitive dysfunction [36]. We observed an increase in ^{18}F-FDG accumulation in the brain tissue of 3xTg-AD mice after rTMS treatment, suggesting an increase in brain glucose metabolism after rTMS, which is conducive to the recovery of neuronal function and the improvement of cognitive function.

High levels of ROS can also alter the local neuronal microenvironment and trigger the release of pro-inflammatory cytokines [31] that exacerbate neuroinflammatory responses [39,40]. Microglia are resident phagocytes of the central nervous system, which play an important role in neurogenesis, tissue maintenance, injury response and pathogen defense [41]. It is a common phenomenon in AD that proliferating and activated microglia accumulate around Aβ plaques [42]. Overactivated microglia can produce a large number of pro-inflammatory cytokines and chemokines, such as IL-6, IL-12, IL-1β, TNF-α, CCL2, express NADPH oxidase, produce ROS and RON, phagocytose synapses results in loss of synapses, and cause neurodegeneration [43–45]. Thus, there is a vicious cycle of mutual activation between inflammation and oxidative stress. Our results showed that the proliferation of microglia in the hippocampal DG region of 6-8-month-old 3xTg-AD mice increased, as well as the levels of pro-inflammatory cytokines IL-6, IL-1β and TNF-α, while rTMS could reduce the activation of microglia in the DG region and reduce the release of pro-inflammatory cytokines. The state of microglia in the CA1 region appears stable, the result is parallel to the number of neurons in the CA1 region. There is a fact that microglia remove unsurvived new neurons during hippocampal neurogenesis in the DG region [41]. It could also be that the ratio of pro- and anti-inflammatory phenotypes of microglia have changed. There is also a literature showing that 20 Hz rTMS can reduce the activation of microglia in the hippocampal DG area and cortex of 5xFAD mice and inhibit the pathological development of AD [46].

Synaptic transmission and plasticity have long been thought to provide a physiological basis for learning, memory, and extensive neural computation. The impairment of synaptic plasticity and the decrease of synapse density are the salient features of early AD [47]. PSD-95 and SYP represent postsynaptic and presynaptic proteins respectively, their levels are reduced in neurodegenerative diseases such as Alzheimer's disease [48]. Postmortem studies showed that the levels of Aβ oligomer and the severity of dementia were related to the level of PSD-95 in AD patients [49]. This study found that rTMS can reverse the reduction of PSD-95 and SYP levels in the hippocampus of 3xTg-AD mice. Autopsy studies also found that the mRNA and protein expression levels of the postsynaptic glutamate receptors NR1, NR2A, and NR2B subunits decreased in AD patients [50]. In this study, it was found that the expression levels of NR1, NR2A and NR2B subunit proteins were down-regulated in the brain of 3xTg-AD mice, while rTMS only increased the level of NR2B, suggesting that rTMS may regulate glutamatergic transmission mainly by regulating NR2B.

Dysregulation of the glutamate system will finally lead to a massive loss of neurons in the brain, the resulting hippocampal atrophy is the most characteristic change in AD [51,52]. Increased GLT-1 expression, alleviation of oxidative stress and neuroinflammation inhibition, etc. can reduce neuron loss and apoptosis [53–55]. Therefore, intervention of the above-mentioned pathological process in the early stage of AD is expected to prevent further development of AD and reverse outcome of cognitive decline. In this study, it was found that after rTMS treatment, the number of Tunel$^+$ cells in the hippocampus of 3xTg-AD mice decreased, the ratio of Bcl2/Bax increased and the number of neurons increased, indicating that rTMS reduced cell loss by reducing apoptosis. rTMS has also been reported to reduce apoptotic cell death and inflammation in remote areas following focal brain injury [56].

It has been reported that high spontaneous glutamate fluctuations can be observed in areas close to Aβ plaques, accompanied by decreased GLT-1 expression, which can be partially restored by ceftriaxone though upregulating GLT-1 expression and activity [57]. Human hippocampal EAAT2 levels decrease at the onset of cognitive dysfunction and are associated with the severity of synaptic degeneration and cognitive impairment in AD patients [6,58]. Literature has shown that GLT-1 expression can be upregulated by PI3K/Akt [12,13], PI3K/Akt is also involved in the regulation of oxidative stress, neuroinflammation, synaptic plasticity, apoptosis, etc. [14,18]. Gene chip analysis showed that GLT-1 expression increased after rTMS [59]. Therefore, we speculate that rTMS can increase glutamate clearance and reduce glutamate excitatory toxicity by activating the PI3K/Akt/GLT-1 pathway. The study found that after rTMS treatment the PI3K/Akt activity in 3xTg-AD mice was increased, the expression of GLT-1 was upregulated, along with the glutamate toxicity was reduced. However, after the administration of PI3K inhibitor LY294002 in 3xTg-AD mice to inhibit PI3K/Akt activity, rTMS could not increase the expression of GLT-1 and failed to improve the cognitive function or reduce neuron loss.

Therefore, we concluded that oxidative stress, glucose metabolism, neuroinflammation, synaptic plasticity and neuron survival were disordered in 3xTg-AD mice. 25 Hz rTMS could reverse the above-mentioned pathological changes by increasing glutamate clearance through the activation of the PI3K/Akt/GLT-1 pathway.

Author contributions

Conceptualization and Design, H.C., C.Z. and F.W.; Methodology, H. C. and Y.H.; Validation, F.W., L.Z.; Data Acquisition, Analysis, and Interpretation: H.C., C.Z., Z.G. and Y.Y.; Writing – Original Draft Preparation H.C. and C.Z.; Writing – Review & Editing, F.W; Project Administration, Y.J.; Funding Acquisition, F.W.

Declaration of competing interest

The authors declare no conflict of interest.

References

[1] Y.J. Chung, B.I. Lee, J.W. Ko, C.B. Park, Photoactive g-C3 N4 nanosheets for light-induced suppression of Alzheimer's beta-amyloid aggregation and toxicity, Adv. Healthcare Mater. 5 (13) (2016) 1560–1565.

[2] S.D. Mhatre, C.A. Tsai, A.J. Rubin, M.L. James, K.I. Andreasson, Microglial malfunction: the third rail in the development of Alzheimer's disease, Trends Neurosci. 38 (10) (2015) 621–636.

[3] Z. Huang, et al., Low-frequency repetitive transcranial magnetic stimulation ameliorates cognitive function and synaptic plasticity in APP23/PS45 mouse model of Alzheimer's disease, Front. Aging Neurosci. 9 (2017) 292.

[4] J.P. Lefaucheur, et al., Evidence-based guidelines on the therapeutic use of repetitive transcranial magnetic stimulation (rTMS): an update (2014-2018), Clin. Neurophysiol. 131 (2) (2020) 474–528.

[5] F.J. Medina-Fernandez, et al., Transcranial magnetic stimulation as an antioxidant, Free Radic. Res. 52 (4) (2018) 381–389.

[6] P. Sompol, et al., Calcineurin/NFAT signaling in activated astrocytes drives network hyperexcitability in abeta-bearing mice, J. Neurosci. 37 (25) (2017) 6132–6148.

[7] C.C. Vittorio Calabrese, T. Albena, Dinkova Kostova, Edward J. Calabrese, Mark P. Mattson, Cellular stress responses, the hormesis paradigm, and vitagenes:novel targets for therapeutic intervention in neurodegenerative disorders, Antioxidants Redox Signal. 13 (11) (2010 Dec 1) 1763–1811.

[8] A. Armada-Moreira, et al., Going the extra (synaptic) mile: excitotoxicity as the road toward neurodegenerative diseases, Front. Cell. Neurosci. 14 (2020) 90.

[9] T.Y. Yang, et al., Alpha-lipoic acid protects against methylmercury-induced neurotoxic effects via inhibition of oxidative stress in rat cerebral cortex, Environ. Toxicol. Pharmacol. 39 (1) (2015) 157–166.

[10] A.M. Sabogal-Guaqueta, et al., Linalool attenuates oxidative stress and mitochondrial dysfunction mediated by glutamate and NMDA toxicity, Biomed. Pharmacother. 118 (2019), 109295.

[11] M.M.S. Benedikt Zott, Wei Hong, Felix Unger, Hsing Jung, Chen-Engerer, Mpf, Bert Sakmann, M. Dominic, A.K. Walsh, A vicious cycle of β amyloid-dependent neuronal hyperactivation, Science 365 (6453) (2019) 559–565.

[12] X. Zhang, et al., Ginsenoside Rd promotes glutamate clearance by up-regulating glial glutamate transporter GLT-1 via PI3K/AKT and ERK1/2 pathways, Front. Pharmacol. 4 (2013) 152.

[13] X. Wu, T. Kihara, A. Akaike, T. Niidome, H. Sugimoto, PI3K/Akt/mTOR signaling regulates glutamate transporter 1 in astrocytes, Biochem. Biophys. Res. Commun. 393 (3) (2010) 514–518.

[14] G. Saw, et al., Epigenetic regulation of microglial phosphatidylinositol 3-kinase pathway involved in long-term potentiation and synaptic plasticity in rats, Glia 68 (3) (2020) 656–669.

[15] H. Xin, et al., MicroRNA cluster miR-17-92 cluster in exosomes enhance neuroplasticity and functional recovery after stroke in rats, Stroke 48 (3) (2017) 747–753.

[16] F. Xu, L. Na, Y. Li, L. Chen, Roles of the PI3K/AKT/mTOR signalling pathways in neurodegenerative diseases and tumours, Cell Biosci. 10 (2020) 54.

[17] S. Gabbouj, et al., Altered insulin signaling in Alzheimer's disease brain - special emphasis on PI3K-Akt pathway, Front. Neurosci. 13 (2019) 629.

[18] H. Li, et al., Neuroprotective effect of phosphocreatine on oxidative stress and mitochondrial dysfunction induced apoptosis in vitro and in vivo: involvement of dual PI3K/Akt and Nrf2/HO-1 pathways, Free Radic. Biol. Med. 120 (2018) 228–238.

[19] Y. Zhuang, et al., Resveratrol attenuates oxidative stress-induced intestinal barrier injury through PI3K/Akt-Mediated Nrf2 signaling pathway, Oxid. Med. Cell. Longev. 2019 (2019), 7591840.

[20] J.H. Yoon, et al., Dieckol ameliorates abeta production via PI3K/Akt/GSK-3beta regulated APP processing in SweAPP N2a cell, Mar. Drugs 19 (3) (2021).

[21] A. Silva, et al., Overexpression of BDNF and full-length TrkB receptor ameliorate striatal neural survival in huntington's disease, Neurodegener. Dis. 15 (4) (2015) 207–218.

[22] P. Sun, et al., Increase in cortical pyramidal cell excitability accompanies depression-like behavior in mice: a transcranial magnetic stimulation study, J. Neurosci. : Off. J. Soc. Neurosci. 31 (45) (2011) 16464–16472.

[23] C. Zuo, et al., Neuroprotective efficacy of different levels of high-frequency repetitive transcranial magnetic stimulation in mice with CUMS-induced depression: involvement of the p11/BDNF/Homer1a signaling pathway, J. Psychiatr. Res. 125 (2020) 152–163.

[24] F. Wang, et al., Improvement of spatial learning by facilitating large-conductance calcium-activated potassium channel with transcranial magnetic stimulation in Alzheimer's disease model mice, Neuropharmacology 97 (2015) 210–219.

[25] K. Tumaneng, et al., YAP mediates crosstalk between the Hippo and PI(3)K–TOR pathways by suppressing PTEN via miR-29, Nat. Cell Biol. 14 (12) (2012) 1322–1329.

[26] H. Tian, et al., Analysis of learning and memory ability in an Alzheimer's disease mouse model using the morris water maze, JoVE 152 (2019).

[27] M. Talantova, et al., Abeta induces astrocytic glutamate release, extrasynaptic NMDA receptor activation, and synaptic loss, Proc. Natl. Acad. Sci. U. S. A. 110 (27) (2013) E2518–E2527.

[28] T.W. Lai, S. Zhang, Y.T. Wang, Excitotoxicity and stroke: identifying novel targets for neuroprotection, Prog. Neurobiol. 115 (2014) 157–188.

[29] R. Wang, P.H. Reddy, Role of glutamate and NMDA receptors in Alzheimer's disease, J. Alzheimers Dis. 57 (4) (2017) 1041–1048.

[30] O. Iyalomhe, et al., The role of hypoxia-inducible factor 1 in mild cognitive impairment, Cell. Mol. Neurobiol. 37 (6) (2017) 969–977.

[31] D.A. Butterfield, The 2013 SFRBM discovery award: selected discoveries from the butterfield laboratory of oxidative stress and its sequela in brain in cognitive disorders exemplified by Alzheimer disease and chemotherapy induced cognitive impairment, Free Radic. Biol. Med. 74 (2014) 157–174.

[32] C. Cheignon, et al., Oxidative stress and the amyloid beta peptide in Alzheimer's disease, Redox Biol. 14 (2018) 450–464.

[33] J. Ai, et al., The neuroprotective effects of phosphocreatine on Amyloid Beta 25-35-induced differentiated neuronal cell death through inhibition of AKT/GSK-3beta/Tau/APP/CDK5 pathways in vivo and vitro, Free Radic. Biol. Med. (2020).

[34] J. Meng, et al., Hydrogen treatment reduces tendon adhesion and inflammatory response, J. Cell. Biochem. (2018).

[35] E. Bouvier, et al., Nrf2-dependent persistent oxidative stress results in stress-induced vulnerability to depression, Mol. Psychiatr. 22 (12) (2017) 1701–1713.

[36] Z. Chen, C. Zhong, Decoding Alzheimer's disease from perturbed cerebral glucose metabolism: implications for diagnostic and therapeutic strategies, Prog. Neurobiol. 108 (2013) 21–43.

[37] S.C. Cunnane, et al., Can ketones compensate for deteriorating brain glucose uptake during aging? Implications for the risk and treatment of Alzheimer's disease, Ann. N. Y. Acad. Sci. 1367 (1) (2016) 12–20.

[38] M. Wiciński, et al., Liraglutide and its neuroprotective properties—focus on possible biochemical mechanisms in alzheimer's disease and cerebral ischemic events, Int. J. Mol. Sci. 20 (5) (2019).

[39] D.A. Butterfield, D. Boyd-Kimball, Oxidative stress, amyloid-beta peptide, and altered key molecular pathways in the pathogenesis and progression of Alzheimer's disease, J. Alzheimers Dis. 62 (3) (2018) 1345–1367.

[40] D.A. Butterfield, B. Halliwell, Oxidative stress, dysfunctional glucose metabolism and Alzheimer disease, Nat. Rev. Neurosci. 20 (3) (2019) 148–160.

[41] T. Kreisel, B. Wolf, E. Keshet, T. Licht, Unique role for dentate gyrus microglia in neuroblast survival and in VEGF-induced activation, Glia 67 (4) (2019) 594–618.

[42] M.W. Salter, B. Stevens, Microglia emerge as central players in brain disease, Nat. Med. 23 (9) (2017) 1018–1027.

[43] D.V. Hansen, J.E. Hanson, M. Sheng, Microglia in Alzheimer's disease, J. Cell Biol. 217 (2) (2018) 459–472.

[44] H. Luo, et al., Apelin-13 suppresses neuroinflammation against cognitive deficit in a streptozotocin-induced rat model of Alzheimer's disease through activation of BDNF-TrkB signaling pathway, Front. Pharmacol. 10 (2019) 395.

[45] H. Sarlus, M.T. Heneka, Microglia in Alzheimer's disease, J. Clin. Invest. 127 (9) (2017) 3240–3249.

[46] K. Li, et al., Early intervention attenuates synaptic plasticity impairment and neuroinflammation in 5xFAD mice, J. Psychiatr. Res. 136 (2021) 204–216.

[47] B. Styr, I. Slutsky, Imbalance between firing homeostasis and synaptic plasticity drives early-phase Alzheimer's disease, Nat. Neurosci. 21 (4) (2018) 463–473.

[48] Y. Liu, et al., Galantamine improves cognition, hippocampal inflammation, and synaptic plasticity impairments induced by lipopolysaccharide in mice, J. Neuroinflammation 15 (1) (2018) 112.

[49] Shichun Tu, Shu-ichi Okamoto, Stuart A. Lipton, H. Xu, Oligomeric Aβ-induced synaptic dysfunction in Alzheimer's disease, Mol. Neurodegener. 9 (48) (2014).

[50] Z. Kristofikova, J. Sirova, J. Klaschka, S.V. Ovsepian, Acute and chronic sleep deprivation-related changes in N-methyl-D-aspartate receptor-nitric oxide signalling in the rat cerebral cortex with reference to aging and brain lateralization, Int. J. Mol. Sci. 20 (13) (2019).

[51] C. Fleitas, et al., proBDNF is modified by advanced glycation end products in Alzheimer's disease and causes neuronal apoptosis by inducing p75 neurotrophin receptor processing, Mol. Brain 11 (1) (2018) 68.

[52] C.Y. Wang, et al., Dl-3-n-Butylphthalide inhibits NLRP3 inflammasome and mitigates alzheimer's-like pathology via nrf2-TXNIP-TrX Axis, Antioxidants Redox Signal. 30 (11) (2019) 1411–1431.

[53] E.E. Spangenberg, et al., Eliminating microglia in Alzheimer's mice prevents neuronal loss without modulating amyloid-beta pathology, Brain 139 (Pt 4) (2016) 1265–1281.

[54] V. Shoshan-Barmatz, E. Nahon-Crystal, A. Shteinfer-Kuzmine, R. Gupta, VDAC1, mitochondrial dysfunction, and Alzheimer's disease, Pharmacol. Res. 131 (2018) 87–101.

[55] H.Y. Gong, et al., Propofol protects hippocampal neurons from apoptosis in ischemic brain injury by increasing GLT-1 expression and inhibiting the activation of NMDAR via the JNK/Akt signaling pathway, Int. J. Mol. Med. 38 (3) (2016) 943–950.

[56] V. Sasso, et al., Repetitive transcranial magnetic stimulation reduces remote apoptotic cell death and inflammation after focal brain injury, J. Neuroinflammation 13 (1) (2016) 150.

[57] J.K. Hefendehl, et al., Mapping synaptic glutamate transporter dysfunction in vivo to regions surrounding Abeta plaques by iGluSnFR two-photon imaging, Nat. Commun. 7 (2016), 13441.

[58] J. Zumkehr, et al., Ceftriaxone ameliorates tau pathology and cognitive decline via restoration of glial glutamate transporter in a mouse model of Alzheimer's disease, Neurobiol. Aging 36 (7) (2015) 2260–2271.

[59] T. Ikeda, S. Kobayashi, C. Morimoto, Effects of repetitive transcranial magnetic stimulation on ER stress-related genes and glutamate, gamma-aminobutyric acid and glycine transporter genes in mouse brain, Biochem. Biophys. Rep. 17 (2019) 10–16.